

PAPER

[View Article Online](#)
[View Journal](#) | [View Issue](#)Cite this: *J. Mater. Chem. A*, 2021, 9, 7190Binding and separation of CO₂, SO₂ and C₂H₂ in homo- and hetero-metallic metal–organic framework materials†Lydia Briggs,^{‡a} Ruth Newby,^{‡b} Xue Han,^a Christopher G. Morris,^{ac} Mathew Savage,^{id a} Cristina Perez Krap,^b Timothy L. Easun,^{id d} Mark D. Frogley,^{id c} Gianfelice Cinque,^{id c} Claire A. Murray,^c Chiu C. Tang,^c Junliang Sun,^{id e} Sihai Yang^{id *a} and Martin Schröder^{id *a}

We report the adsorption of C₂H₂, CO₂ and SO₂ in a new, ultra-stable Cr(III)-based MOF, MFM-300(Cr), {[Cr₂(OH)₂(L)], H₄L = biphenyl-3,3',5,5'-tetracarboxylic acid}. MFM-300(Cr) shows uptakes of 7.37, 7.73 and 8.59 mmol g^{−1} for CO₂, C₂H₂ and SO₂, respectively, at 273 K, 1.0 bar, and shows a higher selectivity for SO₂/CO₂ compared with the Al(III) analogue MFM-300(Al) (selectivity of 79 vs. 45). In order to monitor the effects of changing metal centre on gas uptake and to integrate the properties of the homometallic analogues, the mixed metal MFM-300(Al_{0.67}Cr_{0.33}), [Al_{1.34}Cr_{0.66}(OH)₂(L)] has been synthesised. *In situ* synchrotron micro-FTIR spectroscopy has identified distinct CO₂ binding environments on Al–O(H)–Al, Cr–O(H)–Cr and Al–O(H)–Cr bridges in MFM-300(Al_{0.67}Cr_{0.33}), and we have determined the binding domains for these gases by *in situ* synchrotron X-ray diffraction in both MFM-300(Cr) and MFM-300(Al_{0.67}Cr_{0.33}). The capability of these materials for gas separation has been confirmed by dynamic breakthrough experiments. The incorporation of Al(III) and Cr(III) within the same framework allows tuning of the host–guest and guest–guest interactions within these functional porous materials.

Received 24th January 2021
Accepted 15th February 2021

DOI: 10.1039/d1ta00687h

rsc.li/materials-a

High porosity, chemical and thermal stability and flexible design are critical features of metal–organic framework (MOF) materials. Design-led incorporation of functional groups such as hydroxyl (–OH),^{1–3} amine (–NH₂)^{4,5} and halogen (–F, –Cl, –Br)^{6–8} groups to form supramolecular interactions with guest species is an effective methodology for enhancing gas sorption.^{9,10} The design of MOFs with open metal sites has been explored widely, but this can often lead to materials that are unstable upon desolvation and/or in contact with moisture.^{11,12}

Variation of metal centres in complex structures is a methodology that may alter or enhance materials properties but does not necessarily introduce significant structural changes.¹³ We were thus interested to investigate the properties of mixed-metal MOF materials, and chose Al(III) and Cr(III) as target centres to compare within the MFM-300 series.

Cr(III)-Based MOFs tend to be highly stable and have been used in catalysis.¹⁴ MIL-101(Cr) has removable terminal water molecules connected to a trinuclear [Cr₃(μ₃-O)(O₂CR)₆(–F,OH)(H₂O)₂] building block, leaving two Lewis acidic sites accessible to catalyse a range of reactions such as oxidations and epoxidations.^{15–17} Its extensive use can be attributed to the stability of MIL-101(Cr) to water, and Cr(III)-based MOFs generally show enhanced chemical stability as a result of the low lability of Cr(III), which can also be exploited for gas sorption.^{18,19} The Al(III)-tetracarboxylate MOF, MFM-300(Al), shows high adsorption of CO₂ and SO₂,² while heterometallic MOFs with multiple metal centres within the same framework can show enhanced gas sorption and catalytic capabilities.^{20,21} Herein, we report the synthesis and gas adsorption of two new Cr-containing analogues of MFM-300(Al): the homometallic MFM-300(Cr) and the mixed metal analogue MFM-300(Al_{0.67}Cr_{0.33}). Their capability for gas separation has been studied by IAST analysis²² and by dynamic breakthrough experiments. Synchrotron X-ray powder diffraction has been

^aSchool of Chemistry, University of Manchester, Oxford Road, Manchester, M13 9PL, UK. E-mail: Sihai.Yang@manchester.ac.uk; M.Schroder@manchester.ac.uk

^bSchool of Chemistry, University of Nottingham, University Park, Nottingham, NG7 2RD, UK

^cDiamond Light Source, Harwell Science Campus, Oxfordshire, OX11 0DE, UK

^dSchool of Chemistry, Cardiff University, Cardiff, CF10 3AT, UK

^eCollege of Chemistry and Molecular Engineering, Peking University, Beijing, 100871, China

† Electronic supplementary information (ESI) available: Synthesis procedures, characterization, and additional analysis of crystal structures. Structural data of MFM-300(Al_{1–x}Cr_x) (x = 0, 0.33, 1) derived from powder X-ray diffraction. CCDC 1952013, 1952268, 1952287 and 1952276 for activated MFM-300(Al_{0.67}Cr_{0.33}), CO₂, C₂H₂- and SO₂-loaded structures, respectively, and 1952277, 1952321, 1952320 and 1952280 for activated MFM-300(Cr), CO₂, C₂H₂- and SO₂-loaded structures, respectively. For ESI and crystallographic data in CIF or other electronic format see DOI: 10.1039/d1ta00687h

‡ These authors contributed equally to the work.

used to determine the preferred binding sites for adsorbed CO₂, SO₂ and C₂H₂ within these materials, and synchrotron micro-IR spectroscopy confirms intermolecular interactions of adsorbed gas molecules with M-μ₂O(H)-M' (M and M' = Al or Cr) functionalities. This study reveals new insights into the effects of partial transmetalation in isostructural MOFs on host-guest interactions and overall gas adsorption capacity.

Results and discussion

MFM-300(Cr) was synthesised by hydrothermal reaction of H₄L (biphenyl-3-3'-5-5'-tetracarboxylic acid) and CrCl₃·6H₂O in acidic (HCl) water, and was isolated as blue, microcrystalline powder (yield = 91%). High resolution synchrotron X-ray diffraction confirms that MFM-300(Cr) possesses extended metal chains of [CrO₄(OH)₂] bridged by L⁴⁻ and two *cis*-μ₂-OH groups forming 1D channels that propagate along the *c* axis. The heterometallic MFM-300(Al_{1-x}Cr_x) was synthesised *via* a similar method but using both Al and Cr salts in the reaction to give a light blue microcrystalline powder (yield ~ 86%). Various ratios of Al and Cr salts were tested for synthesis, and the actual Al : Cr ratio within the heterometallic product was determined by ICP-OES analysis (see ESI†). Among all the obtained materials with different ratios, MFM-300(Al_{0.67}Cr_{0.33}) shows the best performance in terms of gas sorption. MFM-300(Al_{0.67}Cr_{0.33}) is isostructural to the parent complexes MFM-300(M) (M = Al, Cr) (Table S3†), with M-OH bond distances of 1.930(1) Å, 1.953(1) Å and 1.868(5) Å in MFM-300(Al), MFM-

300(Cr) and MFM-300(Al_{0.67}Cr_{0.33}), respectively. The homogeneity of the distribution of Cr and Al in MFM-300(Al_{0.67}Cr_{0.33}) has been studied by synchrotron FT-IR experiments. Three bands for ν(OH) are observed at 3690, 3672, and 3641 cm⁻¹ assigned to Al-(OH)-Al, Al-(OH)-Cr and Cr-(OH)-Cr moieties, respectively, thus demonstrating a homogeneous distribution of M(III) centres (Fig. 1d). The ratio of Al : Cr is further confirmed by TGA (Fig. S1†).

Desolvated MFM-300(Cr) and MFM-300(Al_{0.67}Cr_{0.33}) show similar BET surface areas of 1360 and 1305 m² g⁻¹, respectively, and adsorption isotherms for CO₂, C₂H₂ and SO₂ were measured for these materials. At 273 K and 1.0 bar, the total gas uptakes for MFM-300(Al), MFM-300(Cr) and MFM-300(Al_{0.67}Cr_{0.33}) are 7.00, 8.48 and 7.37 mmol g⁻¹ for CO₂, 6.89, 8.67 and 7.73 mmol g⁻¹ for C₂H₂, and 8.1, 10.0 and 8.59 mmol g⁻¹ for SO₂, respectively (Fig. 1a-c). Taking the difference in molecular mass per unit cell into account, the number of gas molecules per metal ion in each MOF is given Table S10.† The thermodynamic parameters *Q*_{st} and Δ*S* were calculated using the van't Hoff isochore (Fig. S6-S11†). With CO₂, C₂H₂ and SO₂ loadings between 0.5–4.0 mmol g⁻¹, the values of *Q*_{st} are 25.5–28.6, 35.0–42.8 and 39.3–46.0 kJ mol⁻¹ for MFM-300(Cr); and 26.4–29.3, 31.5–32.0 and 43.5–54.6 kJ mol⁻¹ for MFM-300(Al_{0.67}Cr_{0.33}), which are similar to those of MFM-300(Al).^{1,2} Ten cycles of adsorption/desorption of SO₂ were conducted for all three materials at 298 K between 0–0.1 bar, and all maintained their full adsorption capacity, confirming their excellent stability under these conditions (Fig. 2a-c). Throughout the

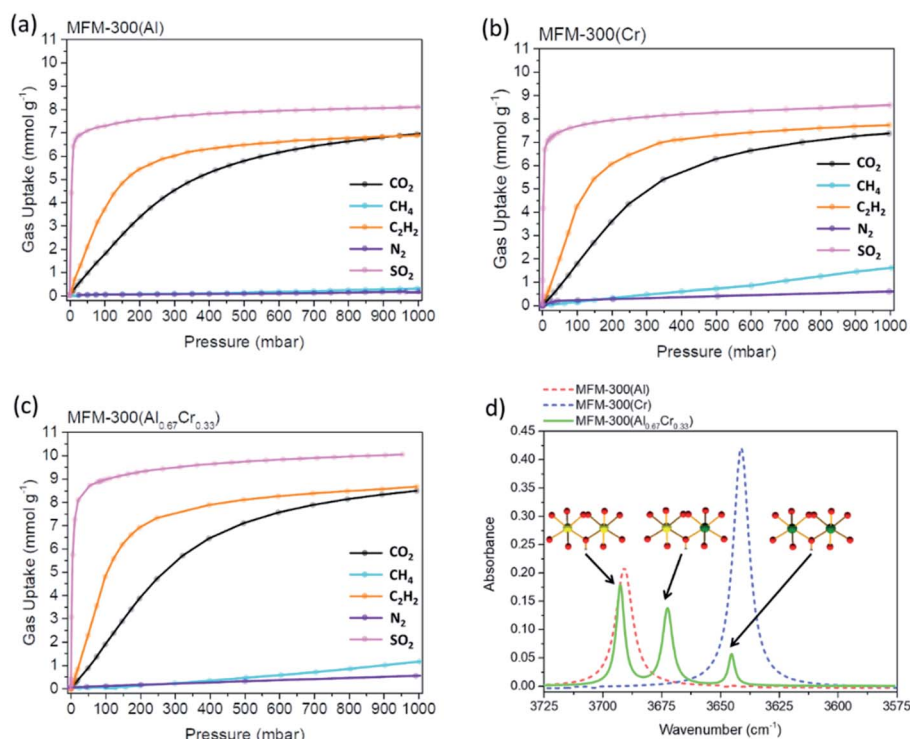


Fig. 1 Adsorption isotherms of CO₂ (black), CH₄ (aqua), C₂H₂ (orange), N₂ (purple) and SO₂ (pink) in (a) MFM-300(Al), (b) MFM-300(Cr) and (c) MFM-300(Al_{0.67}Cr_{0.33}), at 273 K, 0–1 bar; (d) FT-IR spectrum showing the ν(OH) peak in the M–OH–M functionality in MFM-300(Al) (red), MFM-300(Al_{0.67}Cr_{0.33}) (green) and MFM-300(Cr) (blue).



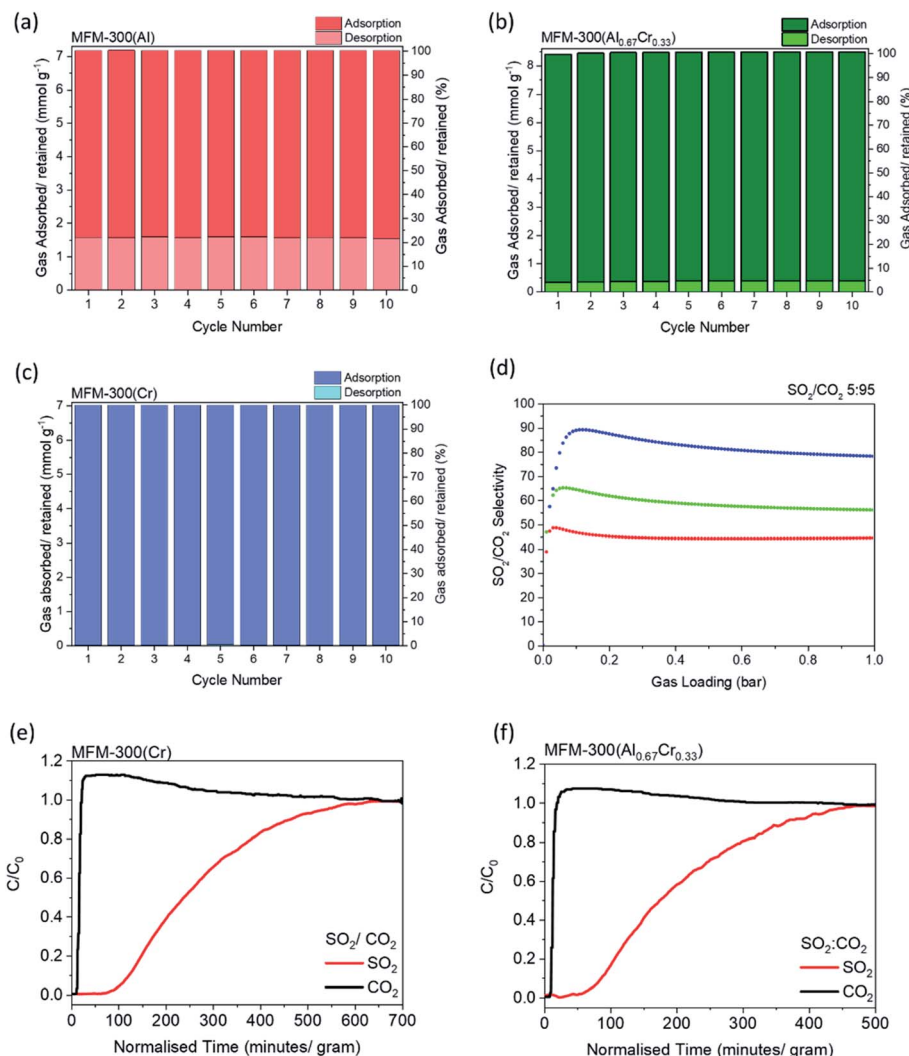


Fig. 2 Cycling experiments of SO_2 at 298 K between 0–0.1 bar in (a) MFM-300(Al), (b) MFM-300($\text{Al}_{0.67}\text{Cr}_{0.33}$) and (c) MFM-300(Cr). (d) IAST selectivity of SO_2/CO_2 (5 : 95) in MFM-300(Al) (red), MFM-300($\text{Al}_{0.67}\text{Cr}_{0.33}$) (green) and MFM-300(Cr) (blue) up to 1 bar at 273 K. Breakthrough plots for SO_2/CO_2 (0.4% SO_2 , 16% CO_2) diluted in He through a fixed bed packed with (e) MFM-300(Cr) and (f) MFM-300($\text{Al}_{0.67}\text{Cr}_{0.33}$) at 298 K and 1 bar.

cycles, MFM-300(Al) and MFM-300($\text{Al}_{0.67}\text{Cr}_{0.33}$) were found to retain SO_2 upon desorption under dynamic vacuum at 298 K (22% and 5% SO_2 retained, respectively), and require elevated temperature to fully remove SO_2 . In contrast, MFM-300(Cr) shows negligible retention of SO_2 (<0.4% or <0.05 mmol g^{-1}) under dynamic vacuum at ambient temperature. Combined with its high structural stability and adsorption capacity, MFM-300(Cr) offers a regenerable platform for SO_2 capture of relevance to flue gas desulfurization.^{23–25} We further explored these MOFs for the separation of SO_2 from CO_2 , as SO_2 is an important flue gas impurity in CO_2 streams and can lead to numerous operational problems in carbon separation and geological sequestration.^{26,27} IAST selectivities of SO_2/CO_2 (5 : 95) were calculated for these MOFs from pure component isotherms between 0–1 bar at 273 K (Fig. 2d). Notably, MFM-300(Cr) shows the highest SO_2/CO_2 selectivity of 79 at 273 K and 1 bar compared to 56 for MFM-300($\text{Al}_{0.67}\text{Cr}_{0.33}$) and 45 for MFM-

300(Al). Dynamic breakthrough experiments with 0.4% SO_2 and 16% CO_2 in He also confirmed the selective retention of low concentrations of SO_2 with MFM-300(Cr) and MFM-300($\text{Al}_{0.67}\text{Cr}_{0.33}$) under flow conditions (Fig. 2e and f). In both cases, CO_2 eluted first and saturated rapidly [$t = 19$ and 21 min g^{-1} for MFM-300($\text{Al}_{0.67}\text{Cr}_{0.33}$) and MFM-300(Cr), respectively], whereas SO_2 starts to elute at $t = 56$ and 76 min g^{-1} , respectively, and shows a steadier breakthrough curve.

To gain deeper understanding of the host–guest interactions underpinning these processes and to rationalise the observed gas selectivities, *in situ* high resolution synchrotron PXRD has been used to determine the preferred binding sites for CO_2 , SO_2 and C_2H_2 molecules within MFM-300(Cr) and MFM-300($\text{Al}_{0.67}\text{Cr}_{0.33}$) via Rietveld refinement (Fig. 3–5; Tables S1 and S2†). For CO_2 , the primary site of adsorption, CO_2^{I} , is bound to the μ_2 -OH group of the hydroxyl-metal chain, $\text{O}^{\mu_2\text{-OH}}\cdots\text{O}^{\text{CO}_2} = 3.301(4), 3.39(1), 3.21(3)$ Å for MFM-300(Cr), MFM-



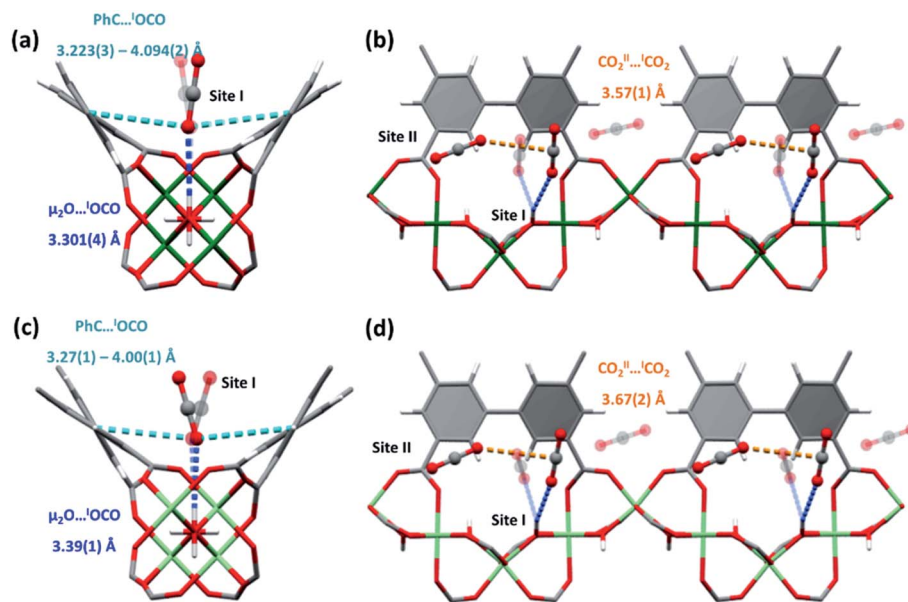


Fig. 3 Views of binding pocket of CO₂^I and CO₂^I...CO₂^{II} interactions in (a and b) MFM-300(Cr) and (c and d) MFM-300(Al_{0.67}Cr_{0.33}). Positionally disordered molecules are shown as translucent. Green: Cr, Light green: AlCr, red: O, grey: C, white: H. Blue bond: μ₂-OH...CO₂^I, turquoise bond: Ph...CO₂^I, orange bonds: CO₂^I...CO₂^{II} interactions.

300(Al_{0.67}Cr_{0.33}) and MFM-300(Al),² respectively, and is disordered by a mirror plane that dissects the μ₂-OH (Fig. 4).^{28,29} CO₂^I is further enclosed by aromatic C–H groups of the biphenyl core of the linker and forms additional supramolecular interactions [O^{CO₂^I}...C^{Aromatic} = 3.223(3)–4.094(2) Å in MFM-300(Cr) and 3.27(1)–4.00(1) Å in MFM-300(Al_{0.67}Cr_{0.33})]. The second site, CO₂^{II}, is positioned near-perpendicular to CO₂^I with full occupancy. The C^{CO₂^I}...O^{CO₂^{II}} distances in MFM-300(Cr), MFM-300(Al_{0.67}Cr_{0.33}) and MFM-300(Al) are 3.57(1), 3.67(2) and 3.92(1) Å, respectively, suggesting a more compact packing of CO₂ in MFM-300(Cr).

For SO₂, two adsorption sites were observed in both MFM-300(Cr) and MFM-300(Al_{0.67}Cr_{0.33}) (Fig. 4). As for CO₂, the primary SO₂ site, SO₂^I, is located with an end-on mode to the bridging μ₂-OH group, O^{μ₂-OH}...O^{SO₂^I} = 3.350(6), 3.163(1) and 3.201(6) Å in MFM-300(Cr), MFM-300(Al_{0.67}Cr_{0.33}) and MFM-300(Al) respectively. SO₂^I also interacts with the surrounding linker moieties *via* van der Waals interactions [O^{SO₂^I}...C^{Aromatic} = 3.08(2)–4.26(7) Å in MFM-300(Cr) and 3.055(2)–3.688(3) Å in MFM-300(Al_{0.67}Cr_{0.33})]. SO₂ at site II is located perpendicularly to SO₂^I with the S^{SO₂^I}...O^{SO₂^{II}} distances being 3.45(3), 3.477(7) and 3.34(7) Å for MFM-300(Cr), MFM-300(Al_{0.67}Cr_{0.33}) and

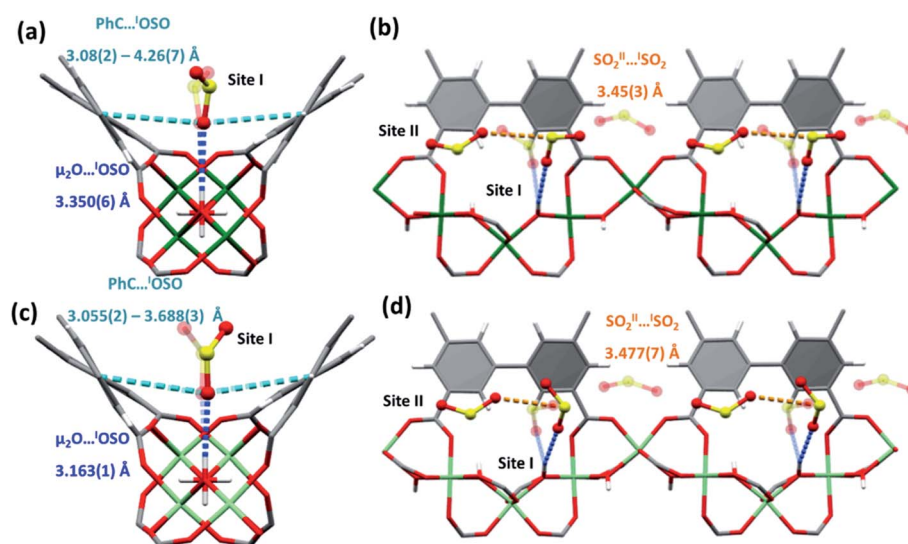


Fig. 4 Views of binding of SO₂^I and of SO₂^I...SO₂^{II} interactions in (a and b) MFM-300(Cr) and (c and d) MFM-300(Al_{0.67}Cr_{0.33}). Positionally disordered molecules are shown as translucent. Green: Cr, light green: AlCr, yellow: S, red: O, grey: C, white: H. Blue bond: μ₂-OH...OSO^I, turquoise bond: Ph...SO₂^I, orange bonds: SO₂^I...SO₂^{II} interactions.



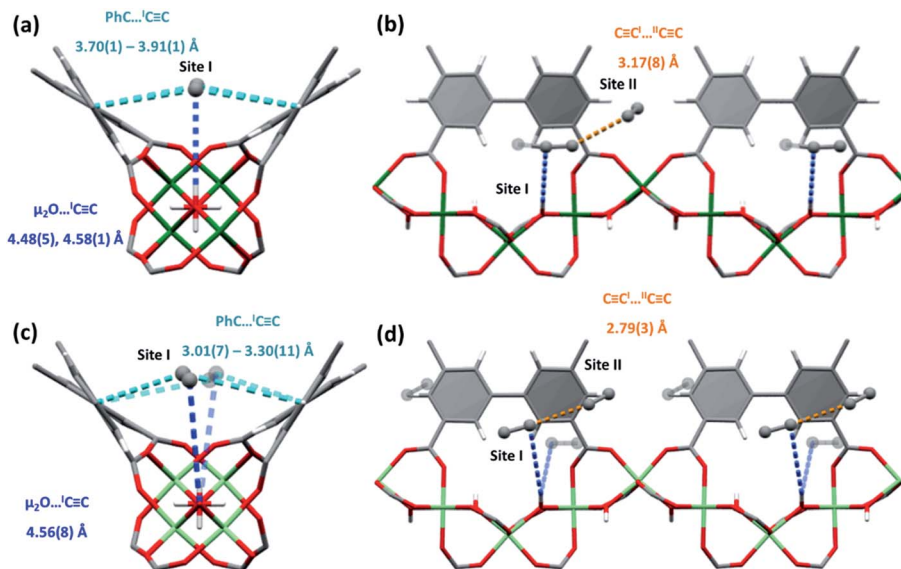


Fig. 5 Views of binding of $C_2H_2^I$ and of $C_2H_2^I \cdots C_2H_2^{II}$ interactions in (a and b) MFM-300(Cr) and (c and d) MFM-300($Al_{0.67}Cr_{0.33}$). Positionally disordered molecules are shown as translucent. Green: Cr, light green: AlCr, red: O, grey: C, white: H. Blue bond: $\mu_2-OH \cdots C \equiv C$, turquoise bond: $Ph \cdots C \equiv C$, orange bonds: $C \equiv C^I \cdots C \equiv C^{II}$ interactions.

MFM-300(Al), respectively. SO_2^{II} also shows weak interactions with the phenyl ring of linker with $S^{O_2} \cdots C^{Aromatic} = 3.53(1)$ and $3.445(3)$ Å, for MFM-300(Cr) and MFM-300($Al_{0.67}Cr_{0.33}$), respectively.

As the bonding distances usually reflect the strength of the host–guest and guest–guest interactions within these system, which often influences the gas selectivities, a summary of bonding distances in CO_2 and SO_2 -loaded MFM-300(Cr), MFM-300($Al_{0.67}Cr_{0.33}$) and MFM-300(Al) is shown in Table 1. When comparing the two single-metal MOFs, MFM-300(Cr) shows weaker bonding interaction to both CO_2 and SO_2 (longer bonding distances) than MFM-300(Al). This reconciles the observed differences in SO_2 residues within these two materials upon desorption at ambient temperature. However, the strong interactions with both CO_2 and SO_2 means that MFM-300(Al) achieves a lower IAST selectivity. The hetero-metallic MFM-300($Al_{0.67}Cr_{0.33}$) exhibits the weakest binding to CO_2 and the strongest binding to SO_2 among these three MOFs. However, the IAST selectivity of SO_2/CO_2 in MFM-300($Al_{0.67}Cr_{0.33}$) falls in between that of the two single-metal MOFs. This strongly suggests that the host–guest bonding distance is not the sole factor to affect the observed selectivity, which will also be influenced by guest–guest interactions. Also, MFM-300($Al_{0.67}Cr_{0.33}$) has a slightly enlarged pore diameter compared

to MFM-300(Al) due to doping with Cr(III), which also likely contributes to the slightly higher gas uptake. In addition, doping MFM-300(Al) with Cr(III) may well form defects leading to increased porosity and additional binding and interaction sites. CO_2 exhibits most compact packing in MFM-300(Cr) (shorter $CO_2 \cdots CO_2$ distance), whereas SO_2 packs most tightly in MFM-300(Al).

For C_2H_2 , two distinct positions of C_2H_2 were observed with both MFM-300(Cr) and MFM-300($Al_{0.67}Cr_{0.33}$) (Fig. 5). $C_2H_2^I$ interacts with the bridging hydroxyl group of MFM-300(Cr) in a side-on manner, and in MFM-300($Al_{0.67}Cr_{0.33}$), $C_2H_2^I$ is slightly off-perpendicular. In both cases, the interactions between the H atom of the hydroxyl to the electron rich $\pi C \equiv C$ in C_2H_2 are weaker than that of CO_2 and SO_2 systems, with longer bonding distances being observed [$HO \cdots C^{C_2H_2^I} = 4.48(5)–4.58(1)$ Å and $4.56(8)$ Å in MFM-300(Cr) and MFM-300($Al_{0.67}Cr_{0.33}$), respectively]. $C_2H_2^I$ is further anchored within a pocket through $\pi \cdots \pi$ stacking interactions with the adjacent phenyl core of the linkers [$C^{C_2H_2^I} \cdots C^{Aromatic} = 3.51(2), 3.73(2), 3.91(1)$ Å in MFM-300(Cr) and $3.01(7), 3.30(11)$ Å in MFM-300($Al_{0.67}Cr_{0.33}$)]. $C_2H_2^{II}$ interacts *via* dipole interactions with $C_2H_2^I$ in a T-shape orientation in MFM-300(Cr) [$C^{C_2H_2^I} \cdots C^{C_2H_2^{II}} = 3.17(8)$ Å], and is more skewed in MFM-300($Al_{0.67}Cr_{0.33}$) but with shorter intermolecular distances [$C^{C_2H_2^I} \cdots C^{C_2H_2^{II}} = 2.79(3)$ Å].

Table 1 Summary of bonding distances within CO_2 and SO_2 -loaded MFM-300(Cr), MFM-300($Al_{0.67}Cr_{0.33}$) and MFM-300(Al)

Bonding distance (Å)	MFM-300(Cr)	MFM-300($Al_{0.67}Cr_{0.33}$)	MFM-300(Al)
$O^{\mu_2-OH} \cdots O^{CO_2}$	3.301(4)	3.39(1)	3.21(3)
$O^{\mu_2-OH} \cdots O^{SO_2}$	3.350(6)	3.163(1)	3.201(6)
$O^{CO_2^I} \cdots O^{CO_2^{II}}$	3.57(1)	3.67(2)	3.92(1)
$O^{SO_2^I} \cdots O^{SO_2^{II}}$	3.45(3)	3.477(7)	3.34(7)



The position of $C_2H_2^{\text{II}}$ is further stabilised by weak van der Waals interactions with the phenyl core of the adjacent linker moieties [$C_2H_2^{\text{II}} \cdots C^{\text{Aromatic}} = 3.97(4), 4.35(7) \text{ \AA}$ and $3.29(13), 3.52(19) \text{ \AA}$ for MFM-300(Cr) and MFM-300($Al_{0.67}Cr_{0.33}$), respectively]. Thus, both MOFs have strong affinity to C_2H_2 through the combined numerous weak interactions which leads to the efficient packing of C_2H_2 within the pores and high C_2H_2 uptake.

To study the dynamics of host-guest binding, *in situ* synchrotron micro-IR spectroscopy was undertaken on MFM-300(Al), MFM-300(Cr) and MFM-300($Al_{0.67}Cr_{0.33}$) as a function of CO_2 loading (Fig. 6). Upon activation under a flow of He, bands for the $\nu(OH)$ stretching modes were observed at 3690 cm^{-1} and 3640 cm^{-1} for MFM-300(Al) and MFM-300(Cr), respectively. In MFM-300(Al), upon increasing the CO_2 partial pressures to 1.0 bar, the Al-O(H)-Al band centred at 3690 cm^{-1} gradually decreases in intensity with a new band growing at 3683 cm^{-1} which is observable from 60% CO_2 loading. This new

peak continues to increase in intensity on additional CO_2 loading. The redshift of 7 cm^{-1} is consistent with the $\mu_2\text{-OH}$ site being increasingly occupied by CO_2 and is consistent with the crystallographic study. In comparison, the $\mu_2\text{-OH}$ peak observed at 3640 cm^{-1} in MFM-300(Cr) undergoes a redshift of 2 cm^{-1} upon increasing CO_2 loading and a significant increase in absorbance intensity. For MFM-300($Al_{0.67}Cr_{0.33}$), distinct absorbance bands for the different $\nu(OH)$ stretching modes were observed at $3692, 3672$ and 3644 cm^{-1} for Al-O(H)-Al, Al-O(H)-Cr and Cr-O(H)-Cr modes, respectively. Upon increasing CO_2 partial pressures to 1 bar, the Al-OH-Al band centred at 3692 cm^{-1} decreases in intensity and a new band at 3683 cm^{-1} emerges. This indicates that the Al-O(H)-Al band is significantly affected by the presence of CO_2 , suggesting a partial depletion of Al-O(H)-Al moieties in the material and CO_2 binding to this moiety. The same is observed for Al-O(H)-Cr with a redshift of 7 cm^{-1} to 3665 cm^{-1} . A shift of 2 cm^{-1} from 3644 to 3642 cm^{-1} is observed in the Cr-O(H)-Cr mode along

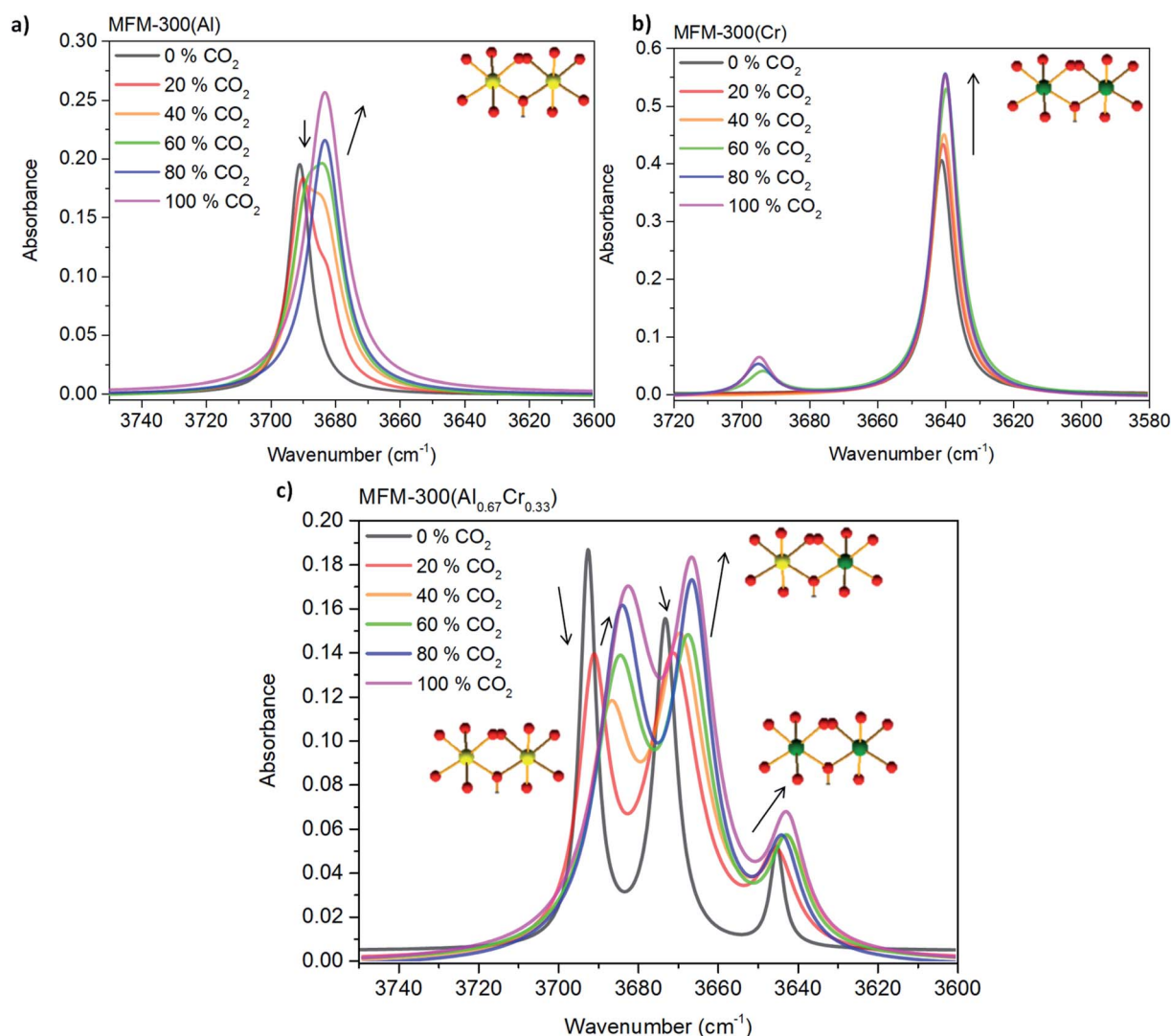


Fig. 6 FTIR spectra of the $\nu(\mu_2\text{-OH})$ stretch region of (a) MFM-300(Al), (b) MFM-300(Cr), and (c) MFM-300($Al_{0.67}Cr_{0.33}$) upon increasing CO_2 loadings from 0 to 100%.



with a broadening of the peak. All $\nu(\text{OH})$ stretching modes were found to shift to lower frequencies upon increasing CO_2 loadings which suggests a weakening of the O–H bond in the metal-hydroxyl moiety consistent with the formation of $\mu_2\text{-OH}\cdots\text{O}=\text{C}=\text{O}$ binding site.

Conclusion

Stable MOFs show increasing promise in the application of capture of toxic gases.²³ The binding domains for CO_2 , SO_2 and C_2H_2 and their host–guest binding dynamics have been studied in a family of three iso-structural MOFs, $\text{MFM-300}(\text{Al}_{1-x}\text{Cr}_x)$ ($x = 0, 0.33, 1$) by *in situ* synchrotron X-ray diffraction and IR micro-spectroscopy. Both $\text{MFM-300}(\text{Al}_{0.67}\text{Cr}_{0.33})$ and $\text{MFM-300}(\text{Cr})$ show enhanced CO_2 , C_2H_2 and SO_2 adsorption uptake than $\text{MFM-300}(\text{Al})$. $\text{MFM-300}(\text{Al}_{0.67}\text{Cr}_{0.33})$ exhibits the highest number of CO_2 , C_2H_2 and SO_2 molecules per metal compared with the homo-metallic analogues, which is likely due to the complex distribution of –OH sites within the pores and the formation of defects *via* doping of $\text{MFM-300}(\text{Al})$ with $\text{Cr}(\text{III})$ leading to increased porosity and additional binding and interaction sites. $\text{MFM-300}(\text{Cr})$ shows the highest SO_2/CO_2 IAST selectivity, which has also been confirmed by breakthrough experiments. $\text{MFM-300}(\text{Cr})$ also promises excellent SO_2 regenerability as confirmed by cycling measurements, demonstrating its potential for selective removal of SO_2 .

Conflicts of interest

The authors declare no competing financial interests.

Acknowledgements

We thank EPSRC (EP/I011870) for support. This project has received funding from the European Research Council (ERC) under the European Union's Horizon 2020 research and innovation programme (grant agreement No 742401, NANOChem). We thank the Royal Society, Peking University and Universities of Nottingham and Manchester for funding. We thank Diamond Light Source for access to Beamlines B22 and I11.

Notes and references

- 1 S. Yang, A. J. Ramirez-Cuesta, R. Newby, V. Garcia-Sakai, P. Manuel, S. K. Callear, S. I. Campbell, C. C. Tang and M. Schröder, *Nat. Chem.*, 2015, **7**, 121–129.
- 2 S. Yang, J. Sun, A. J. Ramirez-Cuesta, S. K. Callear, W. I. F. David, D. P. Anderson, R. Newby, A. J. Blake, J. E. Parker, C. C. Tang and M. Schröder, *Nat. Chem.*, 2012, **4**, 887–894.
- 3 J. Yang, X. Yan, T. Xue and Y. Liu, *RSC Adv.*, 2016, **6**, 55266–55271.
- 4 G. E. Cmarik, M. Kim, S. M. Cohen and K. S. Walton, *Langmuir*, 2012, **28**, 15606–15613.
- 5 R. Vaidhyanathan, S. S. Iremonger, G. K. H. Shimizu, P. G. Boyd, S. Alavi and T. K. Woo, *Science*, 2010, **330**, 650–653.
- 6 S. Noro and T. Nakamura, *NPG Asia Mater.*, 2017, **9**, e433.
- 7 H. Deng, C. J. Doonan, H. Furukawa, R. B. Ferreira, J. Towne, C. B. Knobler, B. Wang and O. M. Yaghi, *Science*, 2010, **327**, 846–850.
- 8 Y. Yuan, J. Li, X. Sun, G. Li, Y. Liu, G. Verma and S. Ma, *Chem. Mater.*, 2019, **31**, 1084–1091.
- 9 X. Lin, I. Telepeni, A. J. Blake, A. Dailly, C. M. Brown, J. M. Simmons, M. Zoppi, G. S. Walker, K. M. Thomas, T. J. Mays, P. Hubberstey, N. R. Champness and M. Schröder, *J. Am. Chem. Soc.*, 2009, **131**, 2159–2171.
- 10 J. Zhang, S. Yao, S. Liu, B. Liu, X. Sun, B. Zheng, G. Li, Y. Li, Q. Huo and Y. Liu, *Cryst. Growth Des.*, 2017, **17**, 2131–2139.
- 11 Y. P. He, Y. X. Tan and J. Zhang, *Cryst. Growth Des.*, 2013, **13**, 6–9.
- 12 T. L. Easun, F. Moreau, Y. Yan, S. Yang and M. Schröder, *Chem. Soc. Rev.*, 2017, **46**, 239–274.
- 13 T. Islamoglu, D. Ray, P. Li, M. B. Majewski, I. Akpınar, X. Zhang, C. J. Cramer, L. Gagliardi and O. K. Farha, *Inorg. Chem.*, 2018, **57**, 13246–13251.
- 14 Q. Guo, L. Ren, P. Kumar, V. J. Cybulskis, K. A. Mkhoyan, M. E. Davis and M. Tsapatsis, *Angew. Chem., Int. Ed.*, 2018, **57**, 4926–4930.
- 15 G. Férey, C. Mellot-Draznieks, C. Serre and F. Millange, *Science*, 2005, **309**, 2040–2042.
- 16 Y. K. Hwang, D. Y. Hong, J. S. Chang, S. H. Jhung, Y. K. Seo, J. Kim, A. Vimont, M. Daturi, C. Serre and G. Férey, *Angew. Chem., Int. Ed.*, 2008, **47**, 4144–4148.
- 17 A. Herbst, A. Khutia and C. Janiak, *Inorg. Chem.*, 2014, **53**, 7319–7333.
- 18 X. Lian, D. Feng, Y.-P. Chen and H. Zhou, *Chem. Sci.*, 2015, **6**, 7044–7048.
- 19 I. J. Kang, N. A. Khan, E. Haque and S. H. Jhung, *Chem.–Eur. J.*, 2011, **17**, 6437–6442.
- 20 D. Sun, F. Sun, X. Deng and Z. Li, *Inorg. Chem.*, 2015, **54**, 8639–8643.
- 21 C. P. Krap, S. Yang, R. Newby, A. Dhakshinamoorthy, H. García, I. Cebula, T. L. Easun, M. Savage, J. E. Eyley, S. Gao, A. J. Blake, W. Lewis, P. H. Beton, M. R. Warren, D. R. Allan, M. D. Frogley, C. C. Tang and M. Schröder, *Inorg. Chem.*, 2016, **55**, 1076–1088.
- 22 J. M. P. A. L. Myers, *AIChE J.*, 1964, **11**, 121–127.
- 23 X. Han, S. Yang and M. Schröder, *Nat. Rev. Chem.*, 2019, **3**, 108–118.
- 24 M. Savage, Y. Cheng, T. L. Easun, J. E. Eyley, S. P. Argent, M. R. Warren, W. Lewis, C. Murray, C. C. Tang, M. D. Frogley, R. T. Murden, M. J. Benham, A. N. Fitch, A. J. Blake, A. J. Ramirez-Cuesta, S. Yang and M. Schröder, *Adv. Mater.*, 2016, **28**, 8705–8711.
- 25 D. Z. Yang, M. Q. Hou, H. Ning, J. Ma, X. C. Kang, J. L. Zhang and B. X. Han, *ChenSusChem*, 2013, **7**, 1191–1195.
- 26 J.-Y. Lee, T. C. Keener and Y. J. Yang, *J. Air Waste Manage. Assoc.*, 2009, **59**, 725–732.
- 27 J. Yu and P. B. Balbuena, *ACS Sustainable Chem. Eng.*, 2015, **3**, 117–124.
- 28 Z. Lu, H. G. W. Godfrey, I. Silva, Y. Cheng, M. Savage, F. Tuna, E. J. L. McInnes, S. J. Teat, K. J. Gagnon,



Paper

M. D. Frogley, P. Manuel, S. Rudic, A. J. Ramirez-Cuesta, S. Yang and M. Schröder, *Nat. Commun.*, 2017, **8**, 14212.
29 M. Savage, Y. Cheng, T. L. Easun, J. E. Eyley, S. P. Argent, M. R. Warren, W. Lewis, C. Murray, C. C. Tang,

M. D. Frogley, R. T. Murden, M. J. Benham, A. N. Fitch, A. J. Blake, A. J. Ramirez-Cuesta, S. Yang and M. Schröder, *Adv. Mater.*, 2016, **28**, 8705–8711.

